Influence of Weight-bearing Portion on Collapse Risk of Femoral Head Necrotic After Intertrochanteric Curved Varus Osteotomy: A Finite Element Analysis

Yuzhu Wang (wangorthopsky@sina.com)
The Fifth Affiliated Hospital of Southern Medical University https://orcid.org/0000-0002-0230-5452
Mincong Wang
The Fifth Affiliated Hospital of Southern Medical University
Chenglong Pan
The Fifth Affiliated Hospital of Southern Medical University

Research Article

Keywords: weight-bearing portion, necrotic collapse risk, finite element analysis

Posted Date: October 20th, 2021

DOI: https://doi.org/10.21203/rs.3.rs-970784/v1

Title: Influence of weight-bearing portion on collapse risk of femoral head necrosis after intertrochanteric curved varus osteotomy: A finite element analysis

Authors: Yuzhu Wang*, Mincong Wang, Chenglong Pan

Department of Orthopaedic Surgery, The Fifth Affiliated Hospital of Southern Medical University, Guangzhou, Guangdong, China.

wangorthopsky@sina.com

Mincong1215@sina.com

pclgjwk@163.com

***Correspondence**: Yuzhu Wang

Department of Orthopaedic Surgery, The Fifth Affiliated Hospital of Southern Medical University, Guangzhou, Guangdong, China.

Tel: 86+15521015656, Email: wangorthopsky@sina.com

Abstract

Background

The influence of the insufficient developmental shape of acetabulum on the collapse occurrence of osteonecrosis of the femoral head (ONFH) was reported rarely after intertrochanteric curved varus osteotomy (CVO). The purpose of the study was to quantitatively evaluate the influence of different weight-bearing portions on collapse risk of femoral head necrosis after CVO with a finite element method.

Methods

Insufficient weight-bearing portion and normal weight-bearing portion hip joint finite element models of CVO (15°, 20°, 25° and 30°) for osteonecrosis of the femoral head with a lesion of 60°, dividing into three types (A, B and C1) were simulated. The Mises strain and collapse index were analyzed in terms of the lesion.

Results

The maximum and mean Mises strain were higher in insufficient weight-bearing portion models with a positive quantitative increment of strain, especially for type C1 and B in no osteotomy situation. However, the collapse index was more than 1.0 in type C1, even after some degree of this CVO, and in type B of insufficient weight-bearing situation.

Conclusions

Progressive collapse risk was increased in the insufficient weight-bearing portion situation. Thus, the decision-making of CVO for the treatment of osteonecrosis of the femoral head should be different with insufficient weight-bearing portion of the

acetabulum. We recommended that the unfavorable biomechanical shape of acetabulum should be treated before this CVO was performed when the necrotic type was more than B.

Keywords: weight-bearing portion, necrotic collapse risk, finite element analysis.

Background

Strategies standing for preserving hip joint for the treatment of osteonecrosis of the femoral head (ONFH) vary based on mechanisms contributed to improving the biological or mechanical characteristics involving in the occurrence of non-hereditary ONFH [1,2,3,4,5,6,7,8,9]. Intertrochanteric curved varus osteotomy (CVO) is one of the proximal femoral osteotomy techniques [10,11,12,13,14]. It is aimed at removing lesions out of the weight-bearing area, decreasing the stress subjected to the infarction to prevent collapse in the early stage, and benefiting from the biomechanically friendly technique widely used in Asia.

The intact ratio measured in an AP radiological view influences the clinical results after CVO. Zhao. et al [15] reported that a post-operative intact ratio of 33.0% was necessary if a satisfactory result was to be achieved after CVO. It has been proved that the stress distribution of the infarction was beneficial from a 30° varus osteotomy to reduce stress levels through much of the necrotic region [14]. It was prone to collapse if located in the anterolateral weight-bearing tract [16], whereas few studies have been investigated the collapse risk factors from the acetabular side (pelvic tilt, center-edge) [17]. Although the necrosis suffered higher stress with less center-edge

angle investigated in our previous study [18]. From a biomechanical point, what influence of different weight-bearing portions on necrosis collapse after CVO is not clear.

In this study, we hypothesized: different weight-bearing portions can affect the biomechanical properties of necrotic bone after CVO, but to what extent is not defined. The purpose of the study was to quantitatively evaluate the influence of different weight-bearing portions on collapse risk of femoral head necrosis after CVO with a finite element method.

Methods

The present study was approved by the Ethical Review Committee of the Fifth Affiliated Hospital of Southern Medical University and involved the examination of an adult volunteer with a informed consent before quantitative computed tomography (QCT) data obtained with the following parameters, slice thickness: 1.0 (mm), voltage: 120 (KV), current: 102.50 (mA), in which a hydroxyapatite (HA) phantom was used during image acquisition to improve the estimation of bone mineral density (BMD) from a volunteer (Sex: male, age: 27 years, Height: 164 cm, Bodyweight: 66kg) without any musculoskeletal disease and operation history of the hip joint (Fig. 1a).

Construction of CVO hip joint 3D models.

The initial hip joint 3D model was constructed from QCT data by segmenting the bony structure of ilium and femur using a medical image processing software

(MIMICS 22, Materialise, Belgium). The interface between the ilium and femoral head was regarded as cartilage geometry, then the cartilage geometry was divided into acetabular and femoral head cartilage (Fig. 1b) [19]. We used the table top plane (TTP) as the referring plane to simulate CVO in this study and the methods described in (Fig. 1c), only the segmented femur solid model was employed to use for determining the osteotomy center (not the femoral head center) and the radius measured with CAD software (SolidWorks 2016, SolidWorks Corp, USA). There were four osteotomy angulations (15°, 20°, 25° and 30°) determined to represent the clinical operations used frequently, then segmented ilium, acetabular cartilage, femoral head cartilage, and necrotic part were assembled to simulate the CVO models without implant fixed.

Definition of necrotic lesion size and type.

CVO for the treatment of ONFH was based on the Japanese Investigation Committee (JIC) classification in which the necrotic lesions were defined based on mechanical character related to the weight-bearing portion of the acetabulum [20]. We used this mechanical JIC classification to simulate three types (A, B, and C1), which was determined in the middle coronal plane of the femoral head, with a fixed size of necrotic lesion that was shaped as a conoid projecting from the femoral head center with the cone angle of 60°to represent an early stage, low risk, precollapse of the lesion [21]. The localization of the lesion was in the middle of the femoral head from the sagittal view, just rotated in the coronal plane, lateral boundary of the three types

of lesions was located in the borderline determined by JIC classification for type A, B, and C1 (Fig. 2).

Generation of CVO finite element models.

The weight-bearing portion varied by modifying the CE angle [22], measured in the middle coronal plane. We determined two different lateral CE angles (18°, 33°) in this study to represent the insufficient weight-bearing portion and normal weight-bearing portion for investigating the influence of the weight-bearing portion on ONFH with CVO (Fig. 3a, 3b). The insufficient weight-bearing portion finite element model (CE angle:18°) was constructed using the methods from the literature page [23]. The normal weight-bearing portion model (CE angle:33°) was the initial configuration of the hip. Finally, a total of 30 different finite-element models simulating three different types of necrosis combined with four varus osteotomies in two different CE angle conditions were established. The mesh type used for all parts in the model was a C3D4 tetrahedron element with the elements of 928,127. The interfaces in the osteotomy were bounded as a tie. The contact of acetabular and femoral head cartilage was defined as no friction.

Material assignment and boundary configurations

The bony structure of the femur was assigned with an isotropy heterogeneous material property based on QCT data, briefly, the parameters used for converting HU to radiographic CT density ($\rho_{QCT}(\mathrm{g/cm^3})$ (*Eq. (1)*) were calculated from B-MAS200 phantom [24], and from ρ_{QCT} to Ash density ($\rho_{ash}(\mathrm{g/cm^3})$ (*Eq. (2)*) [25], then the

apparent density that was calculated from Ash density with a ratio of 0.6 [26] was converted to elastic modulus (*Eq. (3)*) [27].

$$\rho_{QCT}(\mathrm{g/cm^3}) = 0.9863\mathrm{HU} - 2.0804 \quad (1)$$

$$\rho_{ash}(\mathrm{g/cm^3}) = 0.877 \times \rho_{QCT} + 0.0789 \quad (2)$$

$$\mathrm{E} = 6850\rho_{app}^{1.49} \quad (3)$$

Where *Eq. (1), Eq. (2), Eq (3)* were used for calculating the elastic modulus of the femur bone. The material properties of necrosis, cartilage, and ilium were summarized in (Fig. 3).

The boundary configurations were adopted from a validated femoral head necrosis finite element model [28]. A ground reaction force of 700 N for ARCO IIB was performed, seven antagonistic muscles around hip joint were chosen and modeled as axial connectors, of which the loads minimized the internal bending moment in every cross-section of the femur [29], and the loading conditions were present in (Fig. 3). The hip capsular ligaments were attached to the CVO models as 1D springs elements [30,31]. For boundary conditions, the pubic symphysis and sacroiliac joint were fixed to prevent translation and rotation. Finite element analysis for each CVO model was performed using ABAQUS software (ABAQUS 2019, Dassault Systemes, France) in the International Society of Biomechanics (ISB) coordinate system [32].

The Mises strain was used and calculated (*Eq. (4)*, ε_{eqv}: Mises Strain,ε_1: Max strain (LE) ε_2: Mid strain (LE), ε_3: Min strain (LE), ν: Poisson's ratio) for observing the biomechanical

properties changes of necrotic bone differing from the Mises stress. The increment of strain was calculated by values of Mises strain in insufficient weight-bearing portion models minus the values of Mises strain in normal weight-bearing portion models. The collapse index (CI) was also calculated (*Eq. (5)*, ε_{max}: maximum principled strain at each element of the lesion, ε_{lim}: the ultimate strain (ultimate tensile strain ε_{lim} = 0.0073, ultimate compressive strain ε_{lim} = 0.0104)) [33] for evaluating the collapse risk of necrotic bone in different weight-bearing portions along with CVO. The value with 1.0 of CI was regarded as the cut-off point of collapse of necrotic bone.

$$\varepsilon_{eqv} = \frac{1}{1+\nu}\sqrt{\frac{1}{2}\{(\varepsilon_1-\varepsilon_2)^2+(\varepsilon_2-\varepsilon_3)^2+(\varepsilon_3-\varepsilon_1)^2\}} \quad (4)$$

$$CI = \varepsilon_{max} / \varepsilon_{lim} \quad (5)$$

Validation of finite element models

The validation of FE models was performed with sensitivity studies and mesh convergence tests, which was reported clearly in our previous study [18]. Since direct experimental measurements of stress within the necrotic region along the osteotomy model derived from the specimen is difficult to achieve. The physiologic reasonableness and internal consistency must be evaluated for validation from the present model, although the finite element model was simulated by adopting a validated femoral head necrotic model from literature. The present results show physiologically reasonable compressive stress distribution in the medial cortex, tensile stresses in the lateral cortex and in the lateral greater trochanter, and osteotomy interface was compressive stress distribution in the medial and tensile stresses in the

lateral site. For the check of internal consistency, preferential longitudinal compressive-stress transmission through the primary trabeculation system of the femoral head across a coronal head midsection layer was simulated in no necrosis natural model and it was interrupted in the no osteotomy necrosis model, which was consistent with the results of other established studies [14,21,28,34,35].

Results

Mises strain of necrotic bone

The maximum and mean Mises strain of necrotic bone was higher in insufficient weight-bearing models (Fig. 4). Particularly, in no osteotomy situation, the maximum Mises strain was 0.031 vs 0.022 for type C1, 0.018 vs 0.012 for type B. Correspondingly, the stain highlighted in the necrotic bone at the interface of healthy bone, and was weakened along with CVO angle increasing (Fig. 5, 6). For type A, a slight strain increase was observed for insufficient weight-bearing models compared with those of types B and C1 (Fig. 4b, d).

Collapse index of necrotic bone

The collapse index was more than 1.0 in type C1 with less than 25° of the normal weight-bearing models and with less than 20° of the insufficient weight-bearing models. In addition to the situation of type B of no osteotomy insufficient weight-bearing model (Fig. 7). The distribution of collapse index highlighted for type C1 and type B in insufficient weight-bearing models at the interface with healthy bone (Fig. 8, 9).

Discussion

This is the first biomechanical simulation using Mises strain as the mechanical parameter to evaluate the effect of the weight-bearing portion on potential deformation of necrotic bone pre and post CVO. Our main findings were: (1) the Mises strain was higher in insufficient weight-bearing models and decreased along with CVO increasing, respectively, which supported the hypothesis, (2) the collapse index was more than 1.0 in type C1 and type B of insufficient weight-bearing situation, suggesting that higher collapse risk was predicted for clinical practice.

Less weight-bearing portion of acetabulum such as developmental dysplasia of the hip (DDH) can elevate the contact pressure [30]. Because of insufficient contact area from the unfavorable shape of acetabulum, resulting in accelerating degenerative changes of cartilage [36]. Moreover, the possibility of collapse for the lesion increased in the situation of abnormal configurations of the hip [16]. Correspondingly, in this study, the Mises strain was higher in insufficient weight-bearing portion models compared to those normal.

Although CVO decreased the strain level positively, the increment of strain at each osteotomy degree approved that the influence of less weight-bearing area on the necrotic bone did not vanish. This is suggesting that high collapse risk exist although the operations such as CVO were performed in the femur side only if unfavorable

condition of the hip from acetabulum is not improved. The results obtained from finite element analysis was consistent with the clinical research focusing on CVO for ONFH[17], in which CE angle < 25° was one of the factors identified to influence 10 influence 10-year survival(56%) with radiographic failure compared to LCE angle ⩾ 25° with radiographic failure in 10-year survival (77%). Thus, the recommendation of what procedure for the treatment of ONFH is better in the case of the dysplastic acetabulum, whatever, not the CVO as one-way approach.

The types of the lesion were decided in this study based on mechanical characteristics. The effect of the insufficient weight-bearing portion on type C1 was more obvious than type B and A. Interestingly, the max Mises strain increment was negative for type C1 at 30° and type B at 15°, 20°, 25°. The reason maybe was that less load was suffered to the necrotic bone after CVO in insufficient weight-bearing portion models. Such phenomenon featured that local concentrated non-uniform biomechanical distribution (stress, strain) was for the insufficient weight-bearing portion compared to the normal with uniform regular pattern[37].

The location and size of the lesion can influence the collapse risk even after the persevering hip operations[7]. In this study, the collapse index was used for evaluating the influence of weight-bearing portion on collapse risk of the lesion while performing CVO. Although the collapse index was higher in insufficient weight-bearing portion models of type C1, the collapse index of normal models was

more than 1.0 in less than 25° of CVO, in other words, the influence of the location of lesion on collapse risk was more than the insufficient weight-bearing area for type C1. Moreover, the small degree of CVO maybe not enough to eliminate the collapse risk from the predicted results.

The main limitation of the study was a computational simulation of prediction, although consistent with the clinical outcomes, the predicted results cannot be used as a standard for clinical practice. Just providing some suggestions for better decision making. Secondly, this simulation only addressed mechanical factors that would affect the stain distribution of necrotic bone; however, biological factors also need to be considered.

Conclusions

Understanding the complicated interdependence of location of necrotic lesions and the configuration of the hip and pelvis is important in making decisions regarding optimal treatment. This computational simulation suggested progressive collapse risk was increased in the insufficient weight-bearing portion situation, and the location of necrotic bone should be considered before performing persevering hip surgeries for the treatment of ONFH. We recommended that the unfavorable biomechanical shape of acetabulum should be treated before this CVO was performed when the necrotic type was more than B.

Availability of data and materials

The data and materials are available from the corresponding author.

Abbreviations

CVO: Curved varus osteotomy

ONFH: Osteonecrosis of the femoral head

LCE: Lateral center-edge angle

FEA: Finite element analysis

QCT: Quantitative computed tomography

JIC: Japanese Investigation Committee

HU: Hounsfield unit

Eq: Equation

CAD: Computer assisted design

vs: Versus

3D: Three-dimensional

DDH: Developmental dysplasia of the hip

References

1 Wang T, Azeddine B, Mah W, Harvey EJ, Rosenblatt D, Séguin C. Osteonecrosis of the femoral head: genetic basis. Int Orthop, 2019, 43(3): 519-30.

2 Hernigou P, Poignard A, Zilber S, Rouard H. Cell therapy of hip osteonecrosis with autologous bone marrow grafting. Indian J Orthop, 2009, 43(1): 40-5.

3 Steinberg ME, Brighton CT, Steinberg DR, Tooze SE, Hayken GD. Treatment of avascular necrosis of the femoral head by a combination of bone grafting, decompression, and electrical stimulation. Clin Orthop Relat Res, 1984, (186): 137-53.

4 Korompilias AV, Lykissas MG, Beris AE, et al. Vascularised fibular graft in the management of femoral head osteonecrosis: Twenty years later. J Bone J Surg (Br), 2009, 91(3): 287-93.

5 Hernigou P, Beaujean F. Treatment of osteonecrosis with autologous bone marrow grafting. Clin Orthop Reslat Res, 2002, (405): 14-23.

6 Aarvold A, Smith JO, Tayton ER, Jones AM, Dawson JI, Lanham S, Briscoe A, Dunlop DG, Oreffo RO. A tissue engineering strategy for the treatment of avascular necrosis of the femoral head. Surgeon, 2013, 11(6): 319-25.

7 Mont MA, Carbone JJ, Fairbank AC. Core decompression versus nonoperative management for osteonecrosis of the hip. Clin Orthop Reslat Res, 1996, (324): 169-78.

8 Veillette CJ, Mehdian H, Schemitsch EH, McKee MD. Survivorship analysis and radiographic outcome following tantalum rod insertion for osteonecrosis of the femoral head. J Bone J Surg (A), 2006, 88(3): 48-55.

9 Keizer SB, Kock NB, Dijkstra PD, Taminiau AH, Nelissen RG. Treatment of avascular necrosis of the hip by a non-vascularised cortical graft. J Bone J Surg, 2006, 88(4): 460-6.

10 Ito H, Tanino H, Yamanaka Y, Nakamura T, Takahashi D, Minami A, Matsuno T. Long-term results of conventional varus half wedge proximal femoral osteotomy for the treatment of osteonecrosis of the femoral head. J Bone J Surg (Br), 2012, 94(3): 308-14.

11 Lee YK, Park CH, Ha YC, Kim DY, Lyu SH, Koo KH. Comparison of surgical parameter and results between curved varus osteotomy and rotational osteotomy for osteonecrosis of the femoral head. Clin Orthop Surg, 2017, 9(2): 160-168.

12 Sakano S, Hasegawa Y, Torii Y, Kawasaki M, Ishiguro N. Curved intertrochanteric varus osteotomy for osteonecrosis of the femoral head. J Bone J Surg (Br), 2004, 86(3): 359-65.

13 Nozawa M, Enomoto F, Shitoto K, Matsuda K, Maezawa K, Kurosawa H. Rotational Acetabular Osteotomy for Osteonecrosis with Collapse of the Femoral

Head in Yong Patients. J Bone J Surg (A), 2005, 87(3): 514-20.

14 Baker KJ, Brown TD, Brand RA. A finite-element analysis of the effects of intertrochanteric osteotomy on stresses in femoral head osteonecrosis. Clin Orthop Relat Res, 1989, (249): 183-98.

15 Zhao G, Yamamoto T, Ikemura S, Motomura G, Mawatari T, Nakashima Y, Iwamoto Y. Radiological outcome analysis of transtrochanteric curved varus osteotomy for osteonecrosis of the femoral head at a mean follow-up of 12.4 years. J Bone J Surg (Br), 2010, 92(6): 781-6.

16 Roush TF, Olson SA, Pietrobon R, Braga L, Urbaniak JR. Influence of Acetabular Coverage on Hip Survival After Free Vascularized Fibular Grafting for Femoral Head Osteonecrosis. J Bone J Surg (A), 2006, 88(10): 2152-8.

17 Okura T, Hasegawa Y, Morita D, Osawa Y, Ishiguro N. What factors predict the failure of curved intertrochanteric varus osteotomy for the osteonecrosis of the femoral head? Arch. Orthop. Trauma Surg, 2016, 136(12): 1647-55.

18 Wang Y, Yamako G, Okada T, Arakawa H, Nakamura Y, Chosa E. Biomechanical effect of intertrochanteric curved varus osteotomy on stress reduction in femoral head osteonecrosis: a finite element analysis. Biomechanical effect of intertrochanteric curved varus osteotomy on stress reduction in femoral head osteonecrosis: a finite element analysis. J Orthop Surg Res, 2021,23;16(1):465.

19 Henak CR, Carruth ED, Anderson AE, Harris MD, Ellis BJ, Peters CL, Weiss JA. Finite element predictions of cartilage contact mechanics in hips with retroverted acetabula. Osteoarthr Cartil, 2013, 21(10): 1522-9.

20 Sugano N, Atsumi T, Ohzono K, Kubo T, Hotokebuchi T, Takaoka K. The 2001 revised criteria for diagnosis, classification, and staging of idiopathic osteonecrosis of the femoral head. J Orthop Sci, 2002, 7(5): 601-5.

21 Lee MS, Tai CL, Senan V, Shih CH, Lo SW, Chen WP. The effect of necrotic lesion and rotational degree on the stress reduction in transtrochanteric rotational osteotomy for femoral head osteonecrosis – a three-dimensional finite-element simulation. Clin Biomech, 2006, 21(9): 969-76.

22 Wylie JD, Kapron AL, Peters CL, Aoki SK, Maak TG. Relationship Between the Lateral Center-Edge Angle and 3-Dimensional Acetabular Coverage. Orthop J Sport Med, 2017, 5(4): 2325967117700589.

23 Zhao X, Chosa E, Totoribe K, Deng G. Effect of periacetabular osteotomy for acetabular dysplasia clarified by three-dimensional finite element analysis. J Orthop Sci, 2010, 15(5): 632-40.

24 Knowles NK, Reeves JM, Ferreira LM. Quantitative Computed Tomography (QCT) derived Bone Mineral Density (BMD) in finite element studies: a review of the literature. J Exp Orthop, 2016, 3(1): 36.

25 Schileo E, Dall'ara E, Taddei F, Malandrino A, Schotkamp T, Baleani M, Viceconti M. An accurate estimation of bone density improves the accuracy of subject-specific finite element models. J Biomech, 2008, 41(11): 2483-91.

26 Ali AA, Cristofolini L, Schileo E, Hu H, Taddei F, Kim RH, Rullkoetter PJ, Laz PJ. Specimen-specific modeling of hip fracture pattern and repair. J Biomech. 2014 Jan 22;47(2):536-43. doi:Ali AA, Cristofolini L, Schileo E, et al. Specimen-specific modeling of hip fracture pattern and repair. J Biomech, 2014, 47(2): 536-43.

27 Morgan EF, Bayraktar HH, Keaveny TM. Trabecular bone modulus-density relationships depend on anatomic site. J Biomech, 2003, 36(7): 897-904.

28. Zhou GQ, Pang ZH, Chen QQ, et al. Reconstruction of the biomechnical transfer path of femoral head necrosis: A subject-specific finite element investigation. Comput Biol Med, 2014, 52: 96-101.

29 Sverdlova NS, Witzel U. Principles of determination and verification of muscle forces in the human musculoskeletal system: Muscle forces to minimize bending stress. J Biomech, 2010, 43(3): 387-96.

30 Wang X, Peng J, Li D, Zhang L, Wang H, Jiang L, Chen X. Does the optimal position of the acetabular fragment should be within the radiological normal range for all development dysplasia of the hip? A patient-specific finite element analysis. J Orthop Surg Res, 2016, 11(1): 109.

31 Zou Z, Chávez-Arreola A, Mandal P, Board TN, Alonso-Rasgado T.

Optimization of the position of the acetabulum in a ganz periacetabular osteotomy by finite element analysis. J Orthop Res, 2013, 31(3): 472-9.

32 Wu G, Siegler S, Allard P, Kirtley C, Leardini A, Rosenbaum D, Whittle M, D'Lima DD, Cristofolini L, Witte H, Schmid O, Stokes I. ISB recommendation on definitions of joint coordinate system of various joints for the reporting of human joint motion – Part I: Ankle, hip, and spine. J Biomech, 2002, 35(4): 543-8.

33 Xie P, Deng Y, Tan J, Wang M, Yang Y, Ouyang H, Huang W. The effect of rotational degree and routine activity on the risk of collapse in transtrochanteric rotational osteotomy for osteonecrosis of the femoral head—a finite element analysis. Med Biol Eng Comput, 2020, 58(4): 805-14.

34 Li TX, Huang ZQ, Li Y, Xue ZP, Sun JG, Gao HH, He HJ, Chen WH. Prediction of Collapse Using Patient-Specific Finite Element Analysis of Osteonecrosis of the Femoral Head. Orthop Surg, 2019, 11(5): 794-800.

35. Yang JW, Koo KH, Lee MC, Yang P, Noh MD, Kim SY, Kim KI, Ha YC, Joun MS. Mechanics of femoral head osteonecrosis using three-dimensional finite element method. Arch. Orthop Trauma Surg, 2002, 122(2): 88-92.

36. Vafaeian B, Zonoobi D, Mabee M, Hareendranathan AR, El-Rich M, Adeeb S, Jaremko JL. Finite element analysis of mechanical behavior of human dysplasia hip joints: a systematic review. Osteoarthr Cartil, 2017, 25(4): 438-47.

37 Nozomi K, Takehiro I, Kimio S, Komatsu A, Yoichi S. Finite Element Analysis of the Efficacy of Shelf Acetabuloplasty for Acetabular Dysplasia. Int J Phys Med Rehabil, 2018, 6(6): 500.

Acknowledgements

I would like to thank Min-cong Wang for using his valuable time to write the manuscript together and providing a lot of suggestions.

Funding

This work was supported by Research Program of Traditional Chinese Medicine Bureau of Guangdong Province with Grant Number 20202122. The funder had no role in design of the study, the collection, analysis, and interpretation of the data, or in writing the manuscript.

Author information

Affiliations

Department of Orthopaedic Surgery, The Fifth Affiliated Hospital of Southern Medical University, Guangzhou, Guangdong, China.

Yuzhu Wang, Mincong Wang, Chenglong Pan

Contributions

YW and MW contributed to the study equally, as the first co-authors. (I) Conception and design: YW; (II) Administrative support: MW; (III) Provision of study materials or patients: YW; (IV) Collection and assembly of data: MW; (V) Data analysis and interpretation: YW; (VI) Manuscript writing: All authors; (VII) Final approval of manuscript: All authors.

Corresponding author

Correspondence to YW.

Ethics Declarations

Ethics approval and consent to participate

The study was approved by the Ethical Review Committee of Southern Medical University (NO. 21-0223), and informed consent was obtained from subjects.

Consent for publication

Not applicable

Competing interests

The authors declare no conflicts of interest in association with the present study.

Figure legends

Fig. 1 The solid 3D model of CVO. a Parameters of CT data obtained from the subject, b The hip joint model constructed from CT images, c the method of CVO, MFC: medial femoral condyle, LFC: lateral femoral condyle, PF: proximal femur.

Fig. 2 Necrotic simulation using the classification of the Japanese Investigation Committee of Health and Welfare: type A, type B, type C1.

Fig. 3 Finite element models of CVO. a Normal weight-bearing portion model. b Insufficient weight-bearing portion model.

Fig. 4 Maximum (increment) and mean (increment) Mises strain of necrotic bone.

Fig. 5 Mises strain distribution of necrotic bone in top view.

Fig. 6 Mises strain distribution of necrotic bone in central coronal view.

Fig. 7 Maximum collapse index of necrotic bone in each model.

Fig. 8 Collapse index distribution of necrotic bone in top view.

Fig. 9 Collapse index distribution of necrotic bone in central coronal view.

Figures

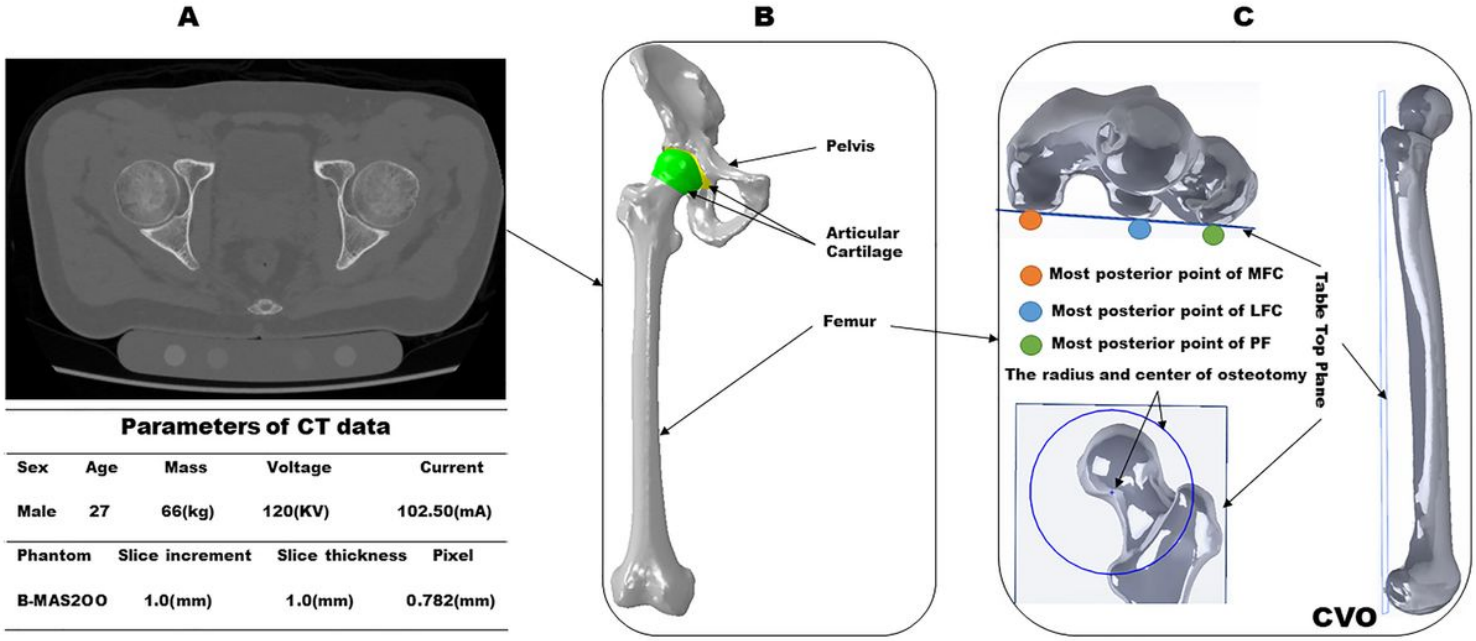

Figure 1

The solid 3D model of CVO. a Parameters of CT data obtained from the subject, b The hip joint model constructed from CT images, c the method of CVO, MFC: medial femoral condyle, LFC: lateral femoral condyle, PF: proximal femur.

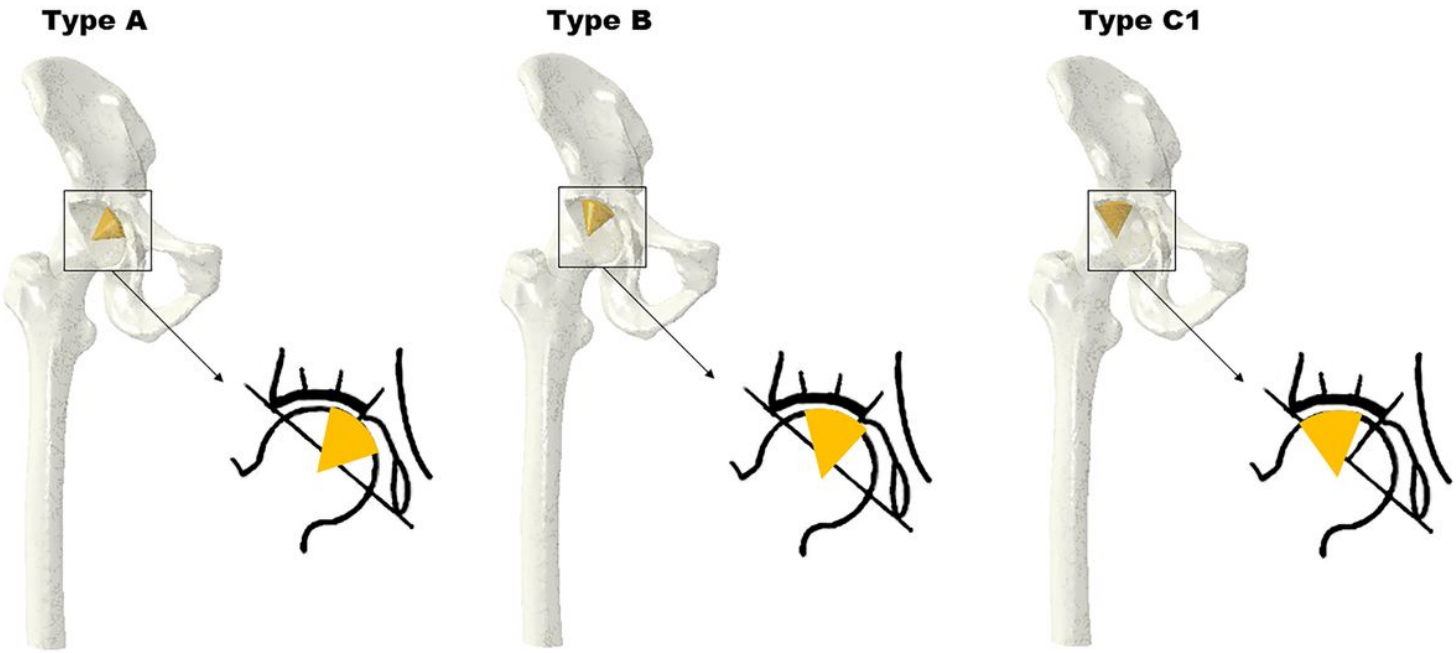

Figure 2

Necrotic simulation using the classification of the Japanese Investigation Committee of Health and Welfare: type A, type B, type C1.

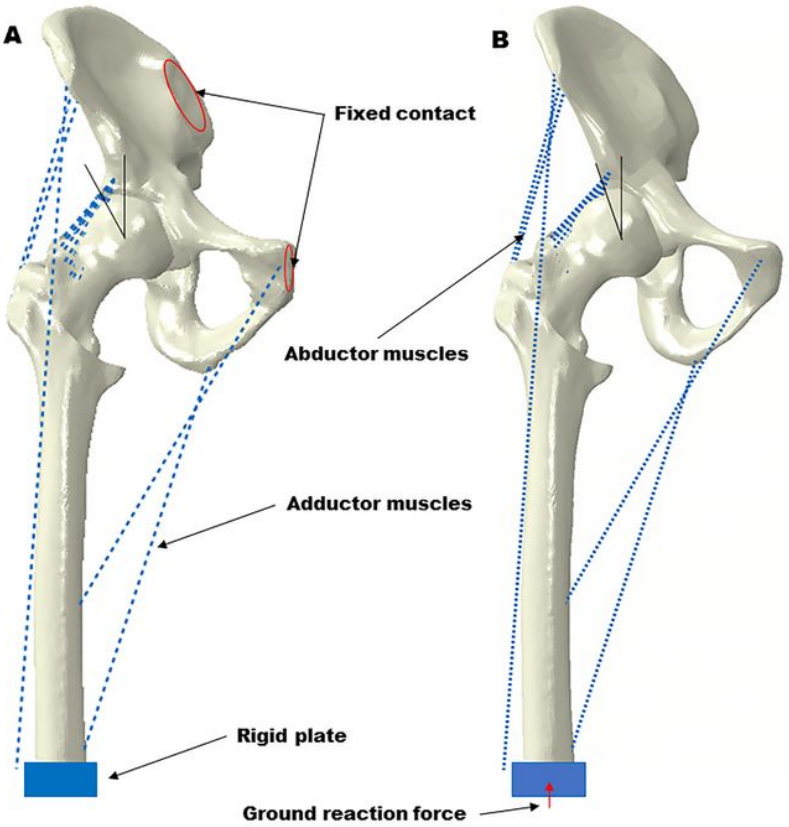

Material properties

Component	Elastic modulus (MPa)	Poisson's ratio
Femur	Isotropic heterogeneous	0.3
Pelvis	Rigid body	
Necrotic bone	124.6	0.152
Cartilage	10.5	0.45

Loading conditions

Component	Forces (N)	Component	Forces (N)
Adductor longus	560	Gluteal minimus	300
Adductor magnus	600	Piriformis	500
Gluteal maximus	550	Tensor fascia latae	300
Gluteal medius	700	Ground reaction force	700

Figure 3

Finite element models of CVO. a Normal weight-bearing portion model. b Insufficient weight-bearing portion model.

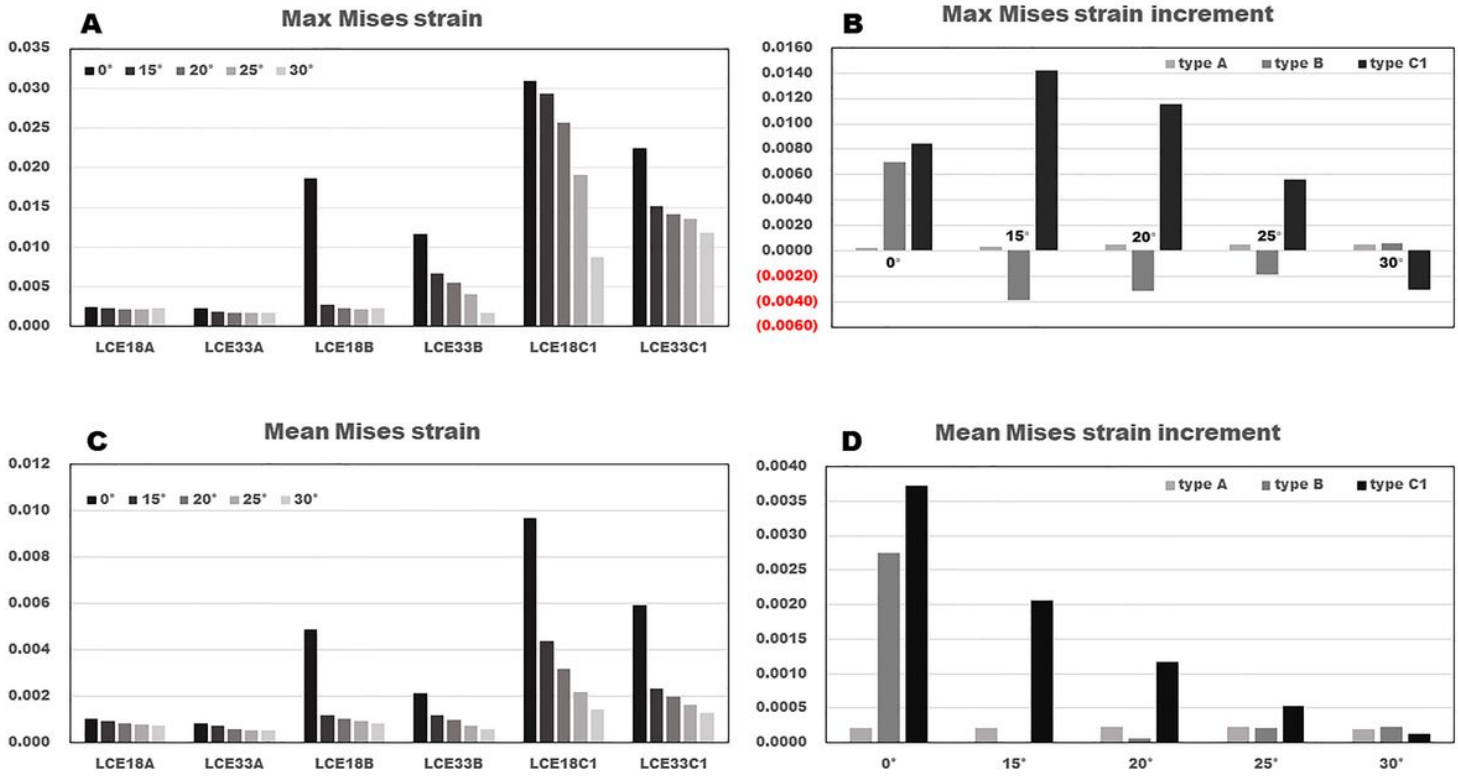

Figure 4

Maximum (increment) and mean (increment) Mises strain of necrotic bone.

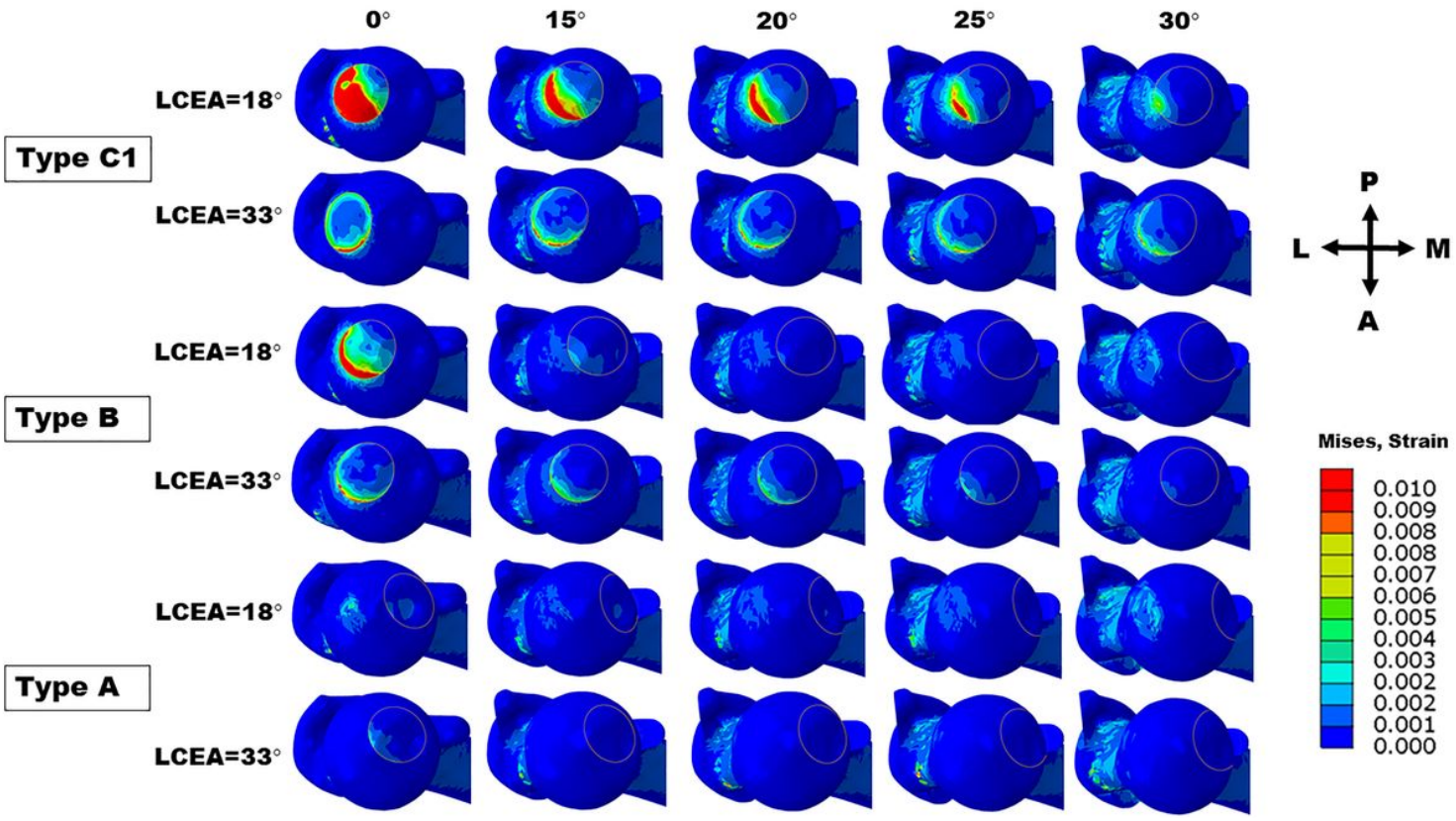

Figure 5

Mises strain distribution of necrotic bone in top view.

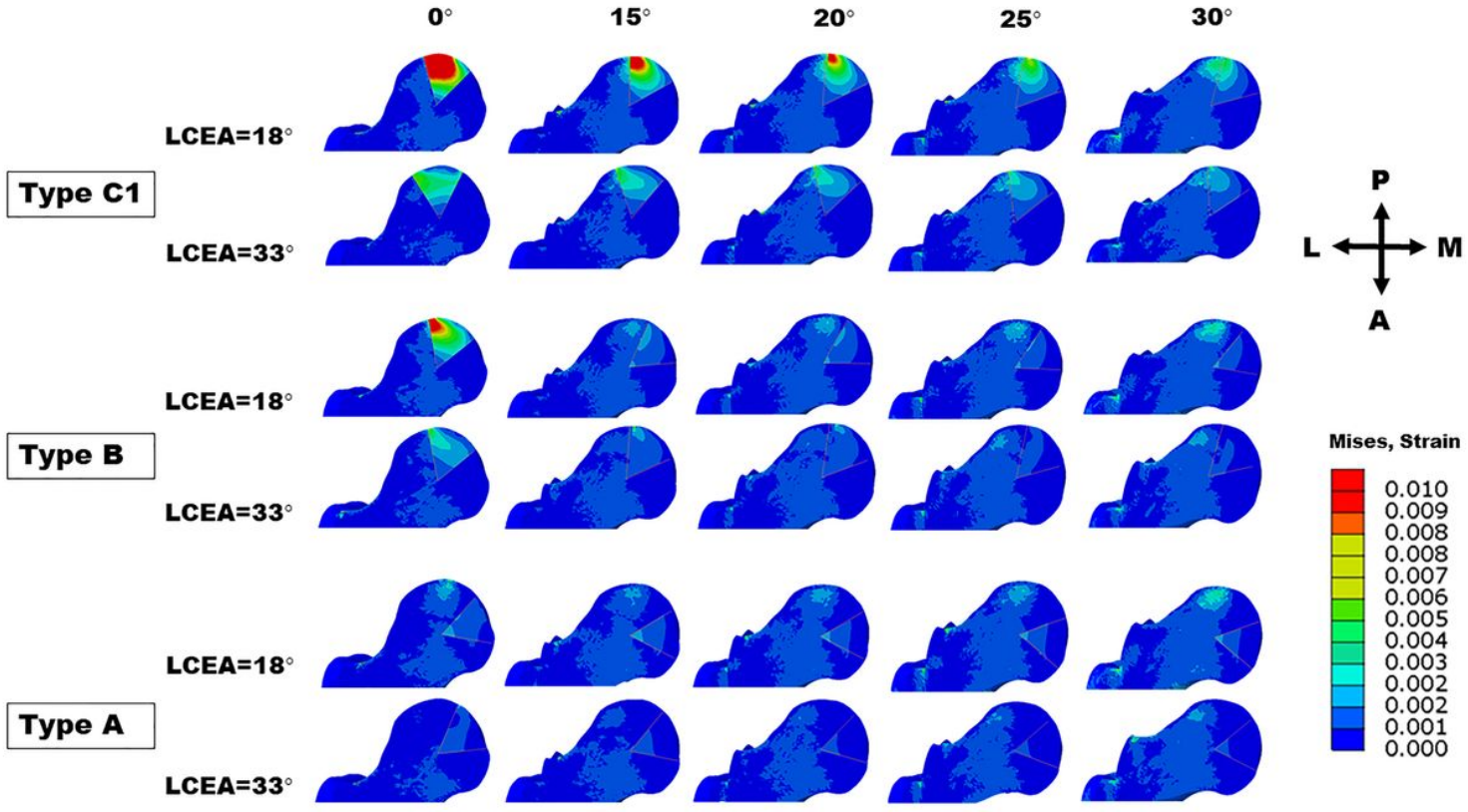

Figure 6

Mises strain distribution of necrotic bone in central coronal view.

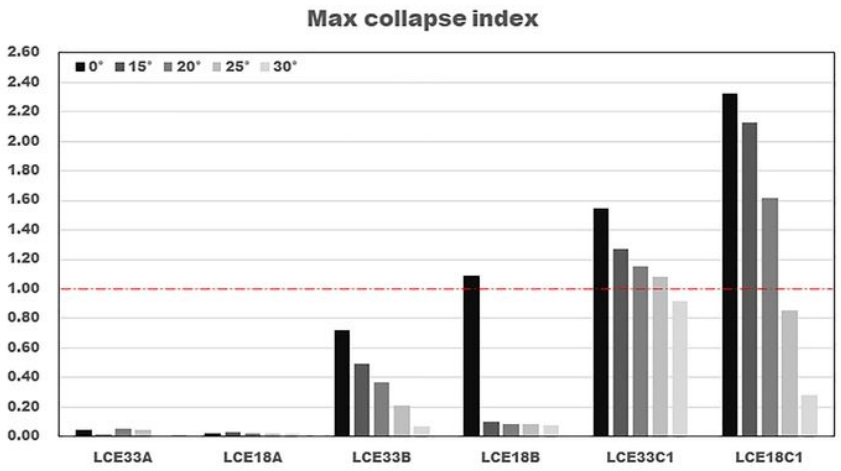

Figure 7

Maximum collapse index of necrotic bone in each model.

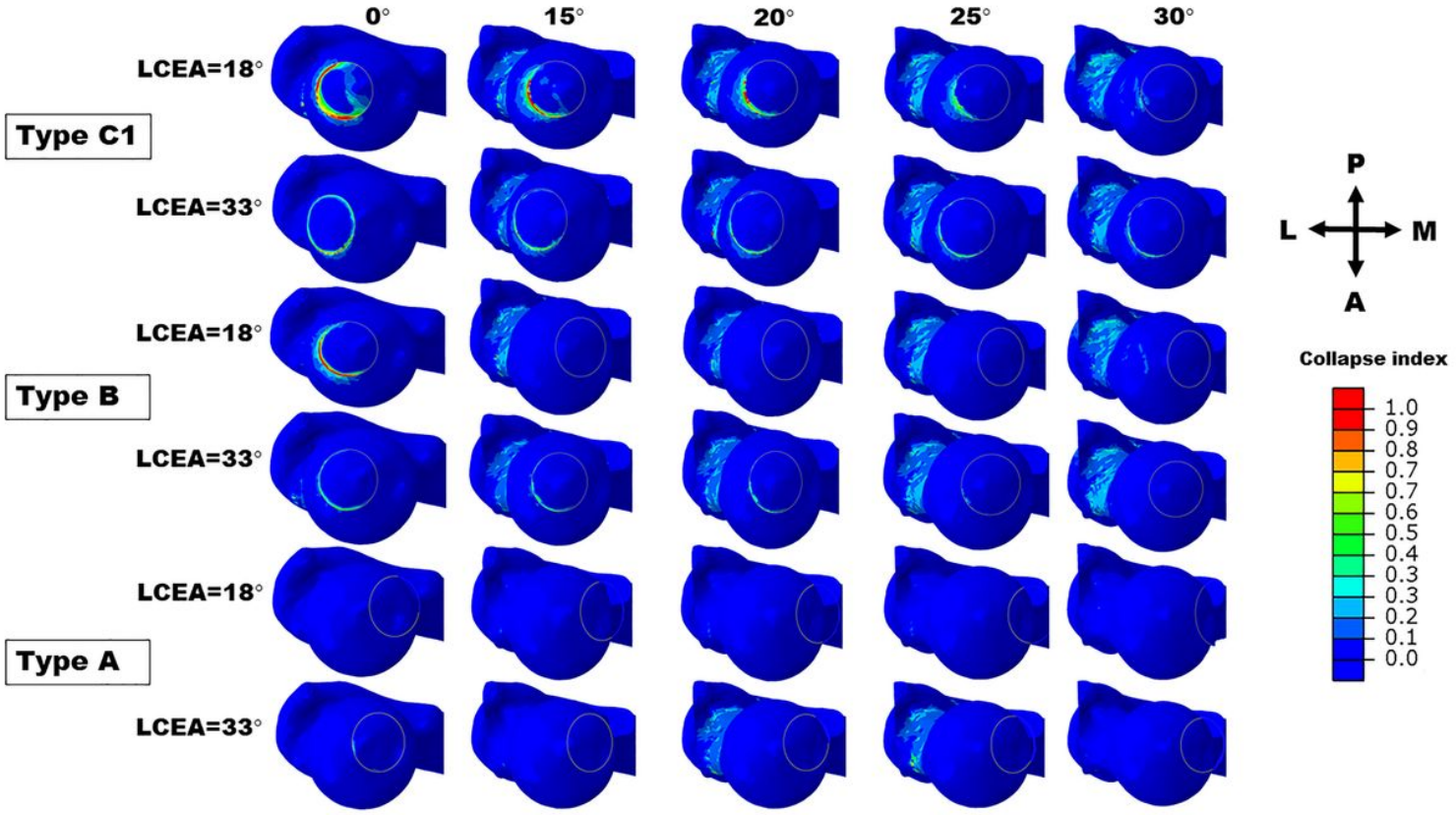

Figure 8

Collapse index distribution of necrotic bone in top view.

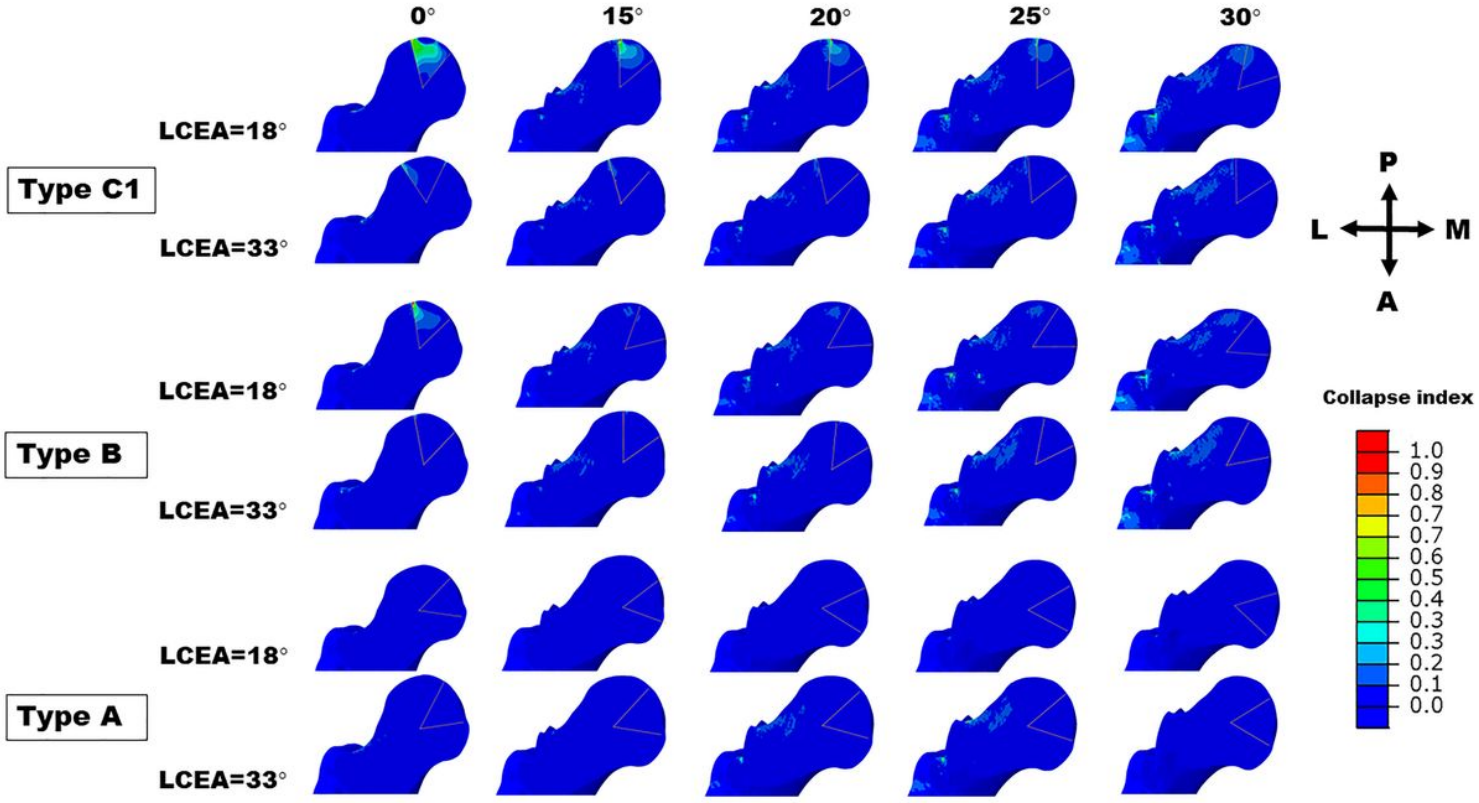

Figure 9

Collapse index distribution of necrotic bone in central coronal view.